RAYLEIGH NUMBER EFFECT ON THE TURBULENT HEAT TRANSFER WITHIN A PARALLELEPIPED CAVITY

by

Mohamed AKSOUH [a*]***, Amina MATAOUI*** [b]***, Nassim SEGHOUANI*** [a]***, and Zoubida HADDAD*** [c]

[a] Department of Astronomy and Astrophysics, Centre of Research of Astronomy Astrophysics and Geophysics – CRAAG, Algiers, Algeria
[b] Theoretical and Applied Laboratory of Fluid Mechanics, University of Science and Technology Houari Boumedienne – USTHB, Algiers, Algeria
[c] University M'hamed Bouguerra, Boumerdes, Algeria

Original scientific paper
UDC: 536.25:532.528:519.217
DOI: 10.2298/TSCI110201114A

This purpose is about a 3-D study of natural convection within cavities. This problem is receiving more and more research interest due to its practical applications in the engineering and the astrophysical research. The turbulent natural convection of air in an enclosed tall cavity with high aspect ratio (Ar = = H/W = 28.6) is examined numerically. Two cases of differential temperature have been considered between the lateral cavity plates corresponding, respectively, to the low and high Rayleigh numbers: Ra = 8.6·10^5 and Ra = = 1.43·10^6. For these two cases, the flow is characterized by a turbulent low Reynolds number. This led us to improve the flow characteristics using two one point closure low-Reynolds number turbulence models: renormalization group k-ε model and shear stress transport k-ω model, derived from standard k-ε model and standard k-ω model, respectively. Both turbulence models have provided an excellent agreement with the experimental data. In order to choose the best model, the average Nusselt number is compared to the experiment and other numerical results. The vorticity components surfaces confirm that the flow can be considered 2-D with stretched vortex in the cavity core. Finally, a correlation between Nusselt number and Rayleigh number is obtained to predict the heat transfer characteristics

Key words: *low-Reynolds number, turbulent natural convection, numerical simulation, rectangular cavity, turbulence modelling, heat transfer*

Introduction

The turbulent natural convection flows are omnipresent in several sciences domain (solar and stellar structure, Earth mantle, atmospheric turbulence, engineering, electronics …), which depends mainly on both the physicochemical properties of the fluids and the geometrical conditions of the configuration. Usually, the natural convection flow, laminar or turbulent,

* Corresponding author; e-mail: aksouhmed@yahoo.fr

is considered by the Rayleigh number, defined by the expression:

$$\mathrm{Ra} = \frac{\mathrm{g}\beta\Delta TW}{a\nu}$$

This work is carried out numerically to study and improve the structure of turbulent natural convection flows within a parallelepiped enclosure. Therefore, heat transfer process has been performed by a large number of theoretical, experimental, and numerically studies. The numerical study of the natural convection in an enclosure becomes more complicated when the configuration is 3-D and with turbulent flow [1]. Special attention will be given in this paper to these both challenges because they often occur in the natural environment and numerous industrial processes. Peng *et al.* [2] performed large eddy simulation (LES) for the same experimental condition of Tian *et al.* [3]. The authors obtained a better agreement between the measured stratification and LES prediction and indicate that 3-D simulations would be more successful in predicting the thermal stratification within the cavity core. Turbulent natural convection in a large air-filled cavity for 3-D and 2-D configuration, Salat *et al.* [4] investigated experimentally and numerically a differentially heated cavity. They observed a good agreement between the experiment and numerical results for the velocity field and of velocity auto-correlations. Nevertheless, discrepancies along the centreline of the thermal stratification and of temperature auto-correlation remain still important. They concluded that introducing experimental temperature measurements in numerical simulations do not answer definitively to the discrepancy observed on the thermal stratification in the cavity core.

In recent numerical works, Gustaven *et al.* [5], Yang *et al.* [6] and Pons [7] examined numerically the 3-D natural convection in tall cavity. Gustaven *et al.* considered a laminar flow of differentially heated air-filled tall cavity with different vertical aspect ratios of 20, 40, and 80 and horizontal aspect ratios of 5 and 0.2. The Nusselt number was correlated for different ratios in order to predict the heat transfer in equipments or building sections. Their computational fluid dynamics (CFD) simulations showed that cavities with horizontal aspect ratio are greater than five could be considered as 2-D for heat transfer rates up to 4%. Except, the velocity and temperature profiles should be 3-D for better precision. Aich *et al.* [8] used the control-volume finite-element method to study numerically the flow field inside a prismatic cavity, their results shows that at the lower Rayleigh number ($\mathrm{Ra} < 10^4$) the diffusion is the dominating heat transfer mechanism whereas at higher Rayleigh number ($\mathrm{Ra} > > 10^5$ and 10^6) buoyancy driven convection is more important. Consequently, the average Nusselt number at the heated wall does not change significantly for the diffusion dominated case whereas it increases rather rapidly with Ra for the convection-dominated case. On the other hand, Yang *et al.* used the direct numerical simulation calculation for unsteady turbulent natural convection with high Rayleigh number in a tall cavity with height-depth-width ratio of 16:8:1. For these conditions, the results showed that the flow becomes turbulent and asymmetric. For experiment work, Betts *et al.* [9] conducted an experimental investigation of turbulent natural convection air-filled-rectangular tall cavity: 0.076 × 2.18 × 0.52 m (corresponding to the width *W*, height *H*, and depth *D*, respectively), where the ratio between the height and the width corresponds to the large aspect ratio: $Ar = H/W = 28.6$. The natural convection flow in the cavity is generated by two differential temperatures between the two vertical lateral plates 19.6 °C and 39.9 °C, where temperature gradient direction is perpendicular to the gravity. Under theses physical and geometrical conditions, the flow in the cavity core becomes fully turbulent with low Reynolds number [9] and the temperature is

stratified [10]. In fact, this paper is the further of our previous work [11], which consisted to study numerically the turbulent natural convection of air in the tall cavity by using two turbulence models: the standard *k-ε* model and its derivative renormalization group (RNG) *k-ε* model. The comparison between the numerical results and the experimental data [11] revealed that the results were suitable for the RNG *k-ε* model compared to its standard model, which is not appropriate for flow at low Reynolds number. However, the aim of this work is to study the same problem by using two low-Re number turbulence models: RNG *k-ε* model [12] and shear stress transport (SST) *k-ω* model [13]. The numerical results for the vertical velocity, the temperature, and the turbulent kinetic energy are compared to the experimental data [9]. In addition, the average Nusselt number along the heated wall is compared to the experiment values of Betts *et al.* [9] and the numerical results of Heish *et al.* [10]. Moreover, the iso-surface of vorticity magnitude shows the generation of the stretched vortex along the tall cavity. The size of this vortex increases with Rayleigh number. The stretched vortex has been confirmed in the literature for slow flow [14]. However, the second objective of this work is to predict the heat transfer *vs.* Rayleigh number evolution. Several works [3, 5, 6, 15-20] predicted a correlation between the average Nusselt number and Rayleigh number for an enclosed cavity for a high cavity aspect ratio. In this paper, we propose a new correlation for a high cavity aspect ratio and a Prandtl number which less than one.

Turbulence models

Mass conservative equation (eq. 1), SRANS (Steady Reynolds average Navier--Stokes) equations (eq. 2) coupled to the averaged energy equation (eq. 3) of the turbulent compressible flows are written as:

– *mass conservative equation*

$$\frac{\partial}{\partial x_i}(\rho u_i) = 0 \tag{1}$$

– *momentum conservation equation*

$$\frac{\partial}{\partial x_i}(\rho u_j u_i) = -\frac{\partial P}{\partial x_i} + \frac{\partial}{\partial x_j}\left[\tau_{ij} - \overline{\rho u_i' u_j'}\right] - \rho g_i \beta (T - T_0) \tag{2}$$

– *energy conservation equation*

$$\frac{\partial}{\partial x_i}(\rho C_p u_j T) = \frac{\partial}{\partial x_j}\left(\kappa \frac{\partial T}{\partial x_j} - \rho C_p \overline{u_j' T'}\right) + P \tag{3}$$

where

$\tau_{ij} = \mu\left(\frac{\partial u_i}{\partial x_j} + \frac{\partial u_j}{\partial x_i}\right) - \frac{2}{3}\mu\left(\frac{\partial u_k}{\partial x_k}\right)\delta_{ij}$ and $P = \tau_{ij}\frac{\partial u_i}{\partial x_j} + \overline{\tau_{ij}'\frac{\partial u_i'}{\partial x_j}}$ is the viscous dissipation.

In these equations, the Reynolds stress component and correlations between the velocity and temperature fluctuations appear which require a closure. The one point closure turbulent models are generally based on the concept of Prandtl-Kolmogorov's turbulent viscosity which is applied in its high Reynolds number form. Thus, the turbulent Reynolds

stress tensor and the correlation of the velocity and temperature fluctuations are deduced using the following algebraic relations (Boussinesq assumption [21]):

$$R_{ij} = -\rho\overline{u_i' u_j'} = \mu_t\left(\frac{\partial u_i}{\partial x_j} + \frac{\partial u_j}{\partial x_i}\right) - \frac{2}{3}\rho\delta_{ij}k \tag{4}$$

$$-\rho\overline{u_i' T'} = \alpha_t \frac{\partial T}{\partial x_i} \tag{5}$$

By analogy with molecular transport, the turbulent Prandtl number for thermal transport can be deduced by:

$$\sigma_t = \frac{\mu_t}{\rho\alpha_t} \tag{6}$$

The Reynolds stresses component and the velocity – temperature correlation appearing, respectively, in the Reynolds equations and the averaged energy equation require to be modelled. Two one point closure turbulence models recommended for low Re number: RNG k-ε model and SST k-ω model have been used in this work.

RNG k-ε model

For near wall turbulence modelling, the RNG methods are recommended for the asymptotic properties of their scales (the space and time fluctuations exist over all scales). On the basis of the scale invariance, inherent characteristic of the critical phenomena, the method allows to obtain systematically the intrinsic properties of the system constituents. RNG methods were initially developed in the context of quantum field theory. Yakhot *et al*. [12] derived from the standard k-ε model the RNG k-ε model using the RNG methods. The equations of the RNG model are summarized as:

– *the turbulence kinetic energy*

$$(\rho k u_i)_{,i} = R_{ij}(u_j)_{,i} + \left[\left(\mu + \frac{\mu_t}{\sigma_k}\right)(k)_{,j}\right]_{,j} - \rho\varepsilon + G_b \tag{7}$$

– *the dissipation rate equation*

$$(\rho\varepsilon)_{,i} = \left[\left(\mu + \frac{\mu_t}{\sigma_\varepsilon}\right)(\varepsilon)_{,j}\right]_{,j} + C_{\varepsilon 1\_RNG}\frac{\varepsilon}{\kappa}[R_{ij}(u_j)_{,i} + G_b] - C_{\varepsilon 2}\rho\frac{\varepsilon^2}{k} - R_\varepsilon \tag{8}$$

$G_b = -\rho g_i \beta\overline{u_i' T'}$ is the production of turbulent kinetic energy due to the buoyancy.

Compared to the standard k-ε model, the additional term in the equation ε is defined:

$$R_\varepsilon = \frac{C_{\mu\_RNG}\rho\eta^3\left(1 - \dfrac{\eta}{\eta_0}\right)}{1 + \alpha_{RNG}\eta^3}\frac{\varepsilon^2}{k} \tag{9}$$

This additional term includes the effect of streamline curvature and provides an analytical derived differential formula for effective viscosity in order to take in accounts the low Reynolds number effect where:

$$\eta = S\frac{k}{\varepsilon}, \quad \eta_0 = 4.38, \quad \alpha_{\mathrm{RNG}} = 0.012, \quad C_{\varepsilon 1\_\mathrm{RNG}} = 1.42, \quad C_{\varepsilon 2\_\mathrm{RNG}} = 1.68$$

$$C_{\mu\_\mathrm{RNG}} = 0.0845, \quad \text{and} \quad \sigma_k = \sigma_\varepsilon = 0.7194$$

The effective viscosity is deduced from the differential equation:

$$\mathrm{d}\left(\frac{\rho^2 k}{\sqrt{\varepsilon\mu}}\right) = 1.72\frac{\hat{\mu}}{\sqrt{\hat{\mu}^3 - 1 + C_{\hat{\mu}}}}\mathrm{d}\hat{\mu} \tag{10}$$

where $\hat{\mu} = \mu_{\mathrm{eff}}/\mu$ and $C_{\hat{\mu}} \approx 100$.

SST k-ω model

Menter [13] developed another turbulence model based on the SST *k-ω* model. The process of the SST method is to use the *k-ω* formulation in the inner zone of the boundary layer and the *k-ε* model in the outer part of the boundary layer. In order to combine these two models, the standard *k-ε* model has been transformed in *k* and *ω* equations, which leads to the introduction of a cross-diffusion term in the dissipation rate equations. The formalism of SST model is summarised as [13, 21]:

– *the turbulence kinetic energy*

$$(\rho k u_i)_{,i} = \left[\left(\mu + \frac{\mu_{\mathrm{t}}}{\sigma_{\mathrm{k}}}\right)k_{,j}\right]_{,j} + \tilde{G}_{\mathrm{k}} - \beta^*\rho\omega k \tag{11}$$

– *the dissipation rate equation*

$$(\rho\omega)_{,i} = \left[\left(\mu + \frac{\mu_t}{\sigma_\omega}\right)\omega_{,j}\right]_{,j} + \frac{\gamma\omega}{k}R_{ij}(u_j)_{,i} - \beta\rho\omega^2 + 2(1-F_1)\rho\sigma_{\omega 2}\frac{1}{\omega}k_{,j}\,\omega_{,j} \tag{12}$$

where $\tilde{G}_{\mathrm{k}} = \min.[R_{ij}(u_j)_{,i}, C_{1\varepsilon}]$ is the generation of turbulence kinetic energy due to mean velocity gradients.

For SST model, the coefficients are expressed in the form:

$$\Phi = F_1\Phi_1 + (1-F_1)\Phi_2 \tag{13}$$

Close to the wall, the blending function F_1 is set to one and zero far from the wall, where:

$$F_1 = \mathrm{tgh}\left(\left\{\min.\left[\max.\left(2\frac{\sqrt{k}}{0.09\omega y}; \frac{500\nu}{y^2\omega}\right), \frac{4\rho k}{\sigma_{\omega 2}D_\omega^+ y^2}\right]\right\}^4\right) \tag{14}$$

and $D_\omega^+ = \max.[(2\rho/\omega\sigma_{\omega 2})k_{,j}\omega_{,j}\cdot 10^{-10}]$

The difference between the standard k-ω model and SST model is, that the term γ is evaluated by eq.13, so $\gamma = F_1\gamma_1 + (1 - F_1)\gamma_2$, where the constants Φ are deduced through Φ_1 from the k-ω model constants and Φ_2 from the k-ε model constants:

for $\Phi 1$

$$\gamma_1 = \frac{\beta_1}{\beta^*} - \frac{\sigma_{\omega 1}\kappa^2}{\sqrt{\beta^*}},\ \sigma_{k1} = 0.85,\ \sigma_{\omega 1} = 0.5,\ \beta_1 = 0.075,\ a_1 = 0.31,\ \beta^* = 0.09,\ \text{and}\ \kappa = 0.41,$$

for $\Phi 2$

$$\gamma_2 = \frac{\beta_2}{\beta^*} - \frac{\sigma_{\omega 2}\kappa^2}{\sqrt{\beta^*}},\ \sigma_{k2} = 1.0,\ \sigma_{\omega 2} = 0.856,\ \beta_2 = 0.0828,\ \beta^* = 0.09,\ \text{and}\ \kappa = 0.41$$

The eddy viscosity is defined by:

$$\mu_t = \frac{\rho a_1 k}{\max.(a_1\omega, \Omega F_2)} \tag{15}$$

where $F_2 = \text{tgh}\left\{\left[\max.\left(2\frac{\sqrt{k}}{0.09\omega y}; \frac{500\nu}{y^2\omega}\right)\right]^2\right\}$.

Numerical procedure

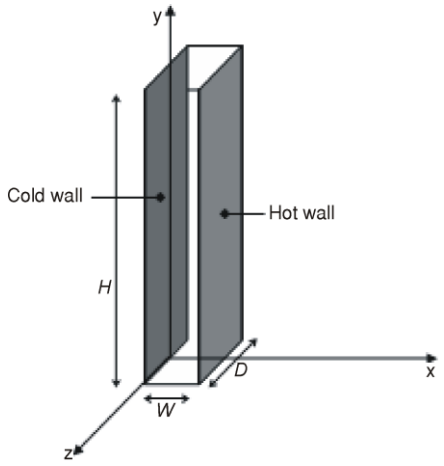

Figure 1. The geometry setting (W = 0.076 m, H = 2.18 m, D = 0.52 m)

We consider an air flow within a tall rectangular cavity with high aspect ratio (Ar = = H/W = 28.68). The dimensions of cavity are 0.076 m × 2.18 m × 0.52 m, as sketched in fig. 1. The spatial derivatives in the equations are solved with the finite volume method [22]. The aim of the finite volume method is to transform the governing equations by the following conservative expression:

$$(\rho u_i \varphi)_{,i} = \left(\Gamma \frac{\partial \varphi}{\partial x_i}\right)_{,i} \tag{16}$$

This equation is transformed in the algebraic equation by the form:

$$a_P \varphi_P^{n+1} = \sum_{nb} a_{nb} \varphi_{nb}^{n+1} + S_\varphi \Delta V + \rho^n \Delta V \varphi_P^n \tag{17}$$

where n is the iteration number and nb is the specification of its neighbour grids (representing north, east, south, west point). Since the flow is steady in average, the SIMPLE algorithm is applied for the pressure-velocity coupling and the power law scheme is use for the interpolation process for all independent variables [23]. The low-Reynolds number turbulence models require refined grid in the inner zone of the boundary layer. The structured mesh has

been used in this study. Different grids sizes have been tested previously [11]. The present numerical results are achieved by 50 × 300 × 50 rectangular non-uniform cells. For the near wall treatment, the enhanced wall function has been applied to specify the turbulence in the near wall region particularly the viscous sublayer. It was also shown that the enhanced wall treatment, which needs a finer mesh in the viscous sublayer, provides more accurate results and perfectly predicts velocity profile within the viscous and buffer layers [24].

For the boundary conditions, two differential temperatures are applied between the lateral plates of 19.6 °C and 39.9 °C, as showing in tab. 1. The front, back, bottom, and top walls were kept adiabatic with no slip condition, $v_x = 0$, $v_y = 0$, and $v_z = 0$.

Table 1. Thermal conditions

	Cold wall	Hot wall	Ra	Pr
1 – First case	15.1 °C	34.7 °C	$0.86 \cdot 10^6$	0.734
2 – Second case	15.6 °C	55.5 °C	$1.43 \cdot 10^6$	0.726

Results and discussion

The vertical velocity and the normal vorticity

At different heights of the cavity for z/D = 0.0, the vertical velocity for both turbulence models are compared with experimental data [9] as shown in figs. 2(a) and 2(b), which correspond to the low and high Rayleigh numbers, respectively. The vertical velocity distributions indicate that the velocity gradient is more significant near the heated walls, with two peaks. Near the hot wall where $T_h > T_m$, the fluid is heated and becomes hot and therefore rises. Fluid from the neighboring areas rushes in to take the place of this rising fluid. On the other hand, near the cold wall ($T_c < T_m$) the plate is cooled and the fluid flows downward. Moreover, in the core region (y/H = 0.5, x/W = 0.5) the figures show that the flow is practically quiescent ($v_y \approx 0$) [25]. The vertical velocity profiles for the two turbulence models are in good agreement compared to the experimental data, with minor discrepancy. However, for more accuracy, in tab. 2 the vertical velocity maximum determined experimentally and numerically by both turbulence models are presented. The error between experimental data and numerical results is expressed as:

$$\text{Error} = \frac{R_{\text{exp.}} - R_{\text{num}}}{R_{\text{num}}} \tag{18}$$

The errors are indicated between the brackets on tab. 2. It should be noted that the vertical velocity maximum determined by SST k-ω model is better than RNG k-ε model. This reveals that the k-ω SST model is more suitable for low Reynolds number turbulent flows.

Furthermore, for natural convection flow the extremum of the vertical velocity in the vicinity to the wall denotes the separation between two layers fig. 2(b) for y/H = 0.5). The first one, is the inner layer which is close to the wall and is dominated by the viscous shear, whereas the second one is the outer layer generated by the turbulent shear with a length until the vertical velocity vanishes ($v_y = 0$). Also, at the mid-width (x/W = 0.5) the vertical velocity profiles show an interaction between the outer layer from the cold wall with outer layer from the hot wall. This interaction is caused by the narrow width of the cavity (W = 0.076 m) in the temperature gradient direction, which produces strong vertical stratification around the cavity

centre and limits the development of turbulent boundary layer along the heated walls. So, two-layer models were developed in order to predict suitable turbulent kinetic energy profiles in order to provide accurate concentrations and temperatures [26].

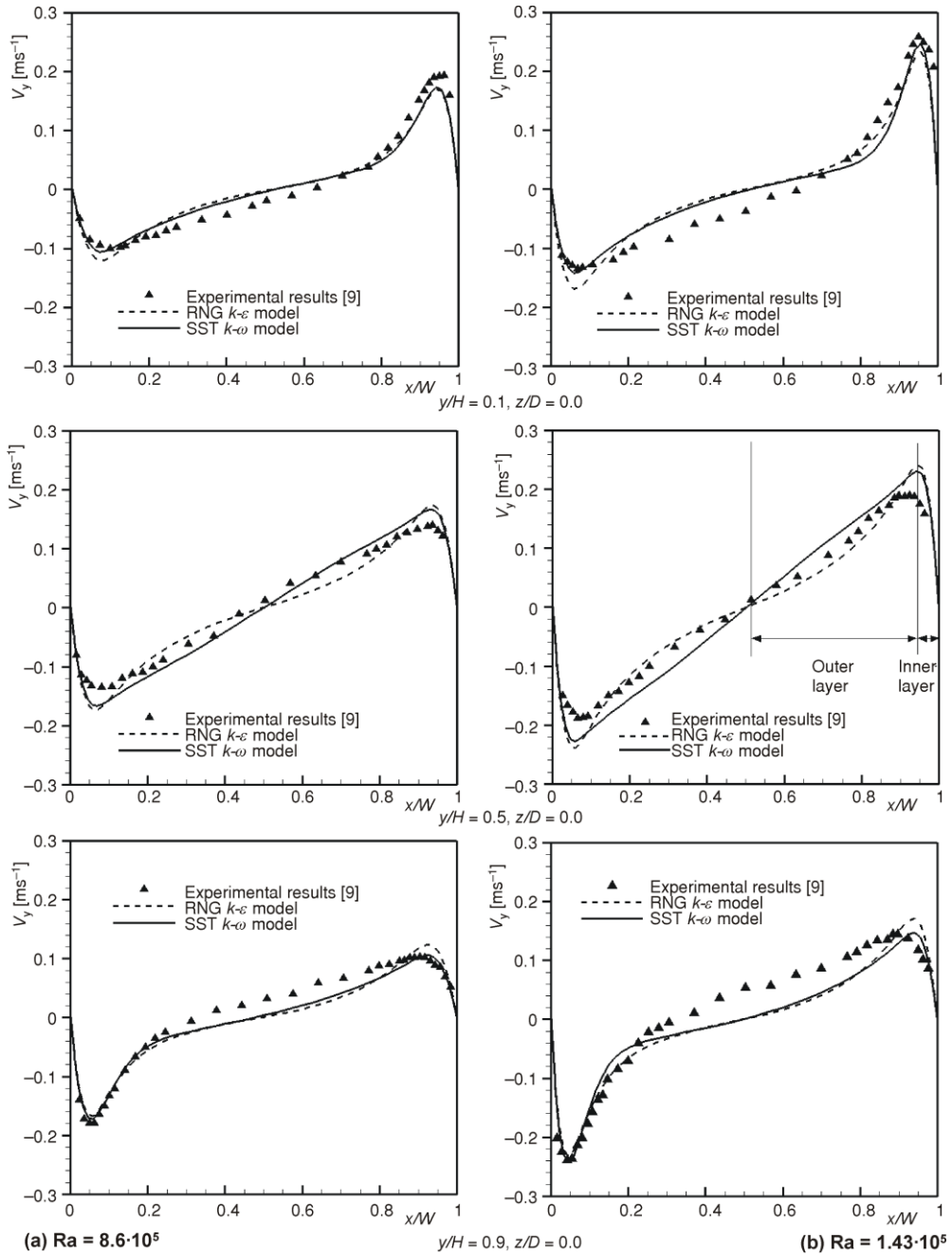

Figure 2. Vertical velocity profiles across the cavity width at various heights for two Rayleigh numbers, for *z/D* = 0.0

Table 2. The maximum and minimum vertical velocities using different turbulence models compared to the experimental data

Ra = $8.6\cdot10^5$						
	$(V_y)_{min.}$			$(V_y)_{max.}$		
	y/H = 0.1	y/H = 0.5	y/H = 0.9	y/H = 0.1	y/H = 0.5	y/H = 0.9
Experiment results [9]	–0.101	–0.135	-0.18	0.193	0.14	0.103
k-ε RNG model	–0.1204 (16.11%)	–0.1732 (22.06%)	–0.1674 (7.53%)	0.1695 (13.86%)	0.1732 (19.17%)	0.1240 (16.94%)
k-ω STT model	–0.1057 (4.45%)	–0.1661 (18.72%)	–0.1729 (4.11%)	0.1728 (11.69%)	0.1661 (15.71%)	0.1060 (2.83%)
Ra = $1.43\cdot10^6$						
	$(V_y)_{min.}$			$(V_y)_{max.}$		
	y/H = 0.1	y/H = 0.5	y/H = 0.9	y/H = 0.1	y/H = 0.5	y/H = 0.9
Experiment results [9]	–0.135	–0.189	–0.239	0.258	0.190	0.145
k-ε RNG model	–0.1690 (20.12%)	–0.2399 (21.22%)	–0.2331 (2.53%)	0.2342 (10.16%)	0.24056 (21.02%)	0.17061 (15.01%)
k-ω STT model	–0.1418 (4.80%)	–0.2280 (17.11%)	–0.2436 (1.89%)	0.2470 (4.45%)	0.2299 (17.36%)	0.1469 (1.29%)

Additionally, the main physical difference between 2-D and 3-D flows is that, in the 2-D case, the vorticity has only one component in the normal direction to the plane of the flow. This imposes a strict constraint on the kinematics and the dynamics of the turbulence [27]. The 3-D study implies that for each point of the flow field, the vorticity vector has three components. The vorticity, which represent the rate of spin of particle fluid, can be defined as the curl of velocity as:

$$\vec{\Omega} = \vec{\nabla} \times \vec{u} \tag{19}$$

Figure 3 illustrates the vorticity components profiles along x/W axis for y/H = 0.5 and z/D = 0.0. Figure 3 highlighted, and confirms [9, 10], that the flow is 2-D with normal vorticity Ω_z, which is perpendicular to the plane of the flow (x, y). Also, this figure proves that the normal vorticity magnitude is optimal near the wall. However, the high vorticity near wall region is generated by shear stress components and not from a swirling or rotational motion.

However, flow patterns determined by the 3-D simulations are more complicated than that of 2-D simulations. Due to the solid edge of boundaries, where the fluid undergoes a buoyancy effect by heat transfer in it from

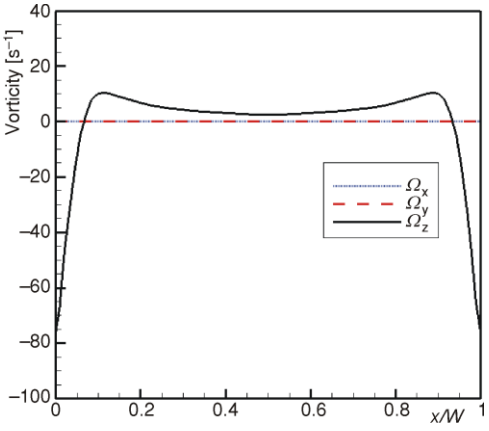

Figure 3. Profile of the vorticity components across the cavity width for y/H = 0.5 and z/D = 0.0, (Ra = $8.6\cdot10^5$)

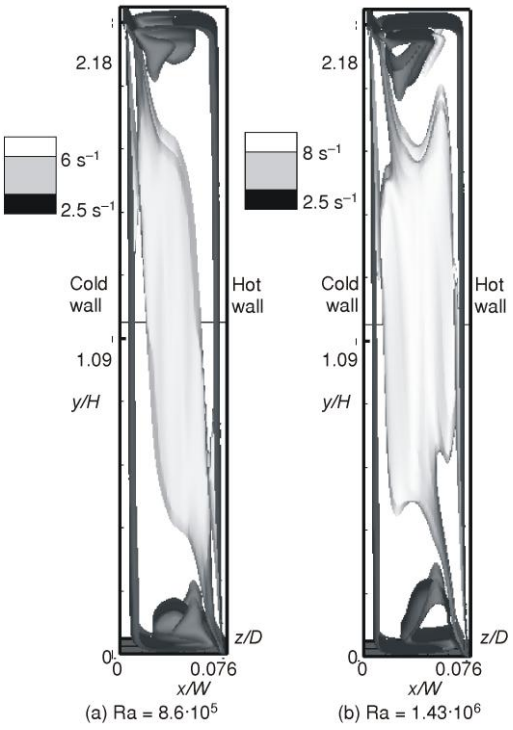

Figure 4. The spanwise normal vorticity iso-surfaces

the end boundaries, the 3-D effects occur and are more important close to the cavity corners probably caused by local temperature gradient. This phenomenon makes the visualization of 3-D a challenge in CFD predictions. Some qualitative features of different vortical structures are often visualized by 3-D simulation by considering the spanwise vorticity component [28]. Figures 4(a) and 4(b) show the normal vorticity iso-surfaces at the level of $\Omega_z = 2.5\ s^{-1}$ and $\Omega_z = 6.0\ s^{-1}$ for $Ra = 8.6 \cdot 10^5$ and at the level of $\Omega_z = 2.5\ s^{-1}$ and $\Omega_z = 8.0\ s^{-1}$ for $Ra = 1.43 \cdot 10^6$. For low Rayleigh number, fig. 4(a) evidences a stretched vortex in the core region with magnitude of $\Omega_z = 6.0\ s^{-1}$. The stretched vortex is confirmed by the literature, which is generated in a flow with low velocity [14]. It can be noticed that when the Rayleigh number increases, fig. 4(b), and when the flow is still done at low velocity, the magnitude and scale of the stretched vortex are expanded. Furthermore, the second iso-surface of the normal vorticity with magnitude $\Omega_z = 2.5\ s^{-1}$, and less than stretched vortex, is in the vicinity of the top cold wall and the bottom hot wall, close to the cavity corners. The 2-D simulations do not predict the visualisation of these vortexes. The flow pattern shows an excellent symmetry with respect to centre of the cavity, indicating that the heat transfer rate from the heated vertical wall should be identical to the cooling vertical wall. Also, when the thermal gradient increases, the flow is accelerated in these zones leading to increase the vortex scale.

The turbulent kinetic energy

The experiment [9] does not provide data of normal fluctuating velocity *w*', since it is very difficult to estimate w' for the anisotropic turbulent natural convection without direct measurement. Therefore, to compare the turbulent kinetic energy *k* evolution between different numerical methods and experiment, eq. 20 has been used in order to deduce *k* thought the experimental data:

$$k = \frac{1}{2}(\overline{u_i' u_i'}) \tag{20}$$

Figures 5(a) and 5(b) illustrate the streamwise profiles of the turbulent kinetic energy (at $y/H = 0.5$ and $z/D = 0.0$). For the fluctuating values, the both turbulence models reproduce practically numerical results compared to the experimental data. However, for the 3-D study, the normal fluctuating velocity values *w*' are not negligible, than the turbulent kinetic energy is underestimated experimentally. In the core of the cavity ($x/W = 0.5$), the

turbulent kinetic energy is high inversely to the vertical velocity which is practically zero (fig. 2) and where this zone is considered as the outer layer of boundary layer. These figures show clearly that the level of turbulent kinetic energy increase with Rayleigh number. Besides, for high Ra number, the experimental values are more underestimated by the increase of *w*'.

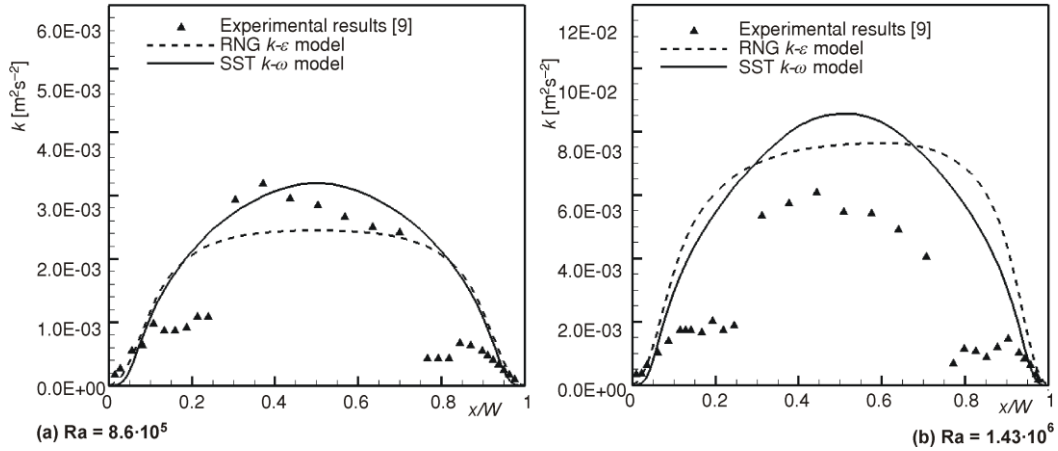

Figure 5. Evolution of the turbulent kinetic energy, across the cativy (*y/H* = 0.5, *z* = 0)

The temperature evolutions and the heat transfer

The mean temperatures profiles for both low and high Rayleigh numbers are plotted in figs. 6(a) and 6(b), respectively. The numerical results are in good agreement with experimental data for the RNG *k*-*ε* and the SST *k*-*ω* models. Similarly, to the mean vertical velocity evolution, the mean temperature shows strong gradients close to the wall with an almost linear variation in the cavity core. Xaman *et al.* [19] explain this result by the heat conduction through the central core of the layer in addition to the heat transport by natural convection. Furthermore, in the vicinity to the wall, the temperature evolution is linear characterising the conductive and viscous sublayers.

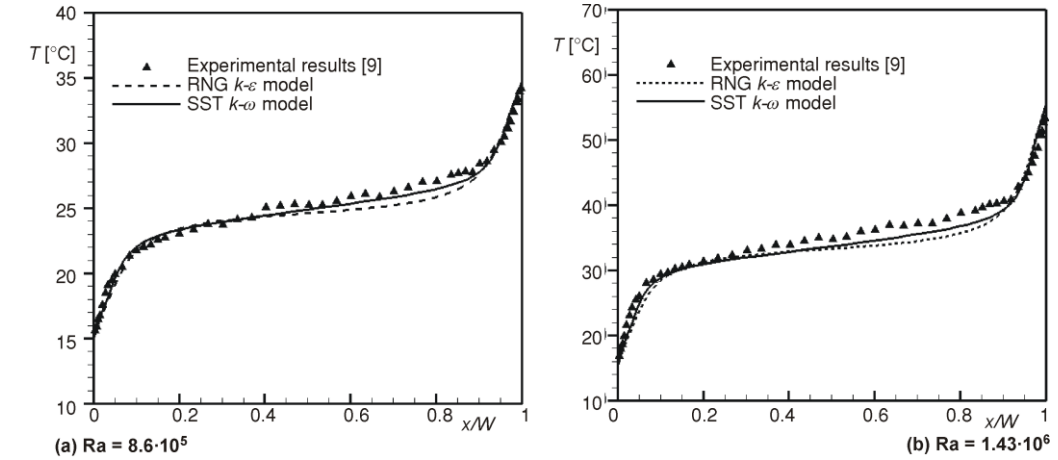

Figure 6. Temperature profile cross the cavity for the low and the high Rayleigh number (*y/H* = 0.5, *z* = 0)

However, the heat transfer along the heated wall is calculated using Nusselt number, which characterizes the ratio of convective to conductive heat transfer across the corresponding boundary:

$$\mathrm{Nu} = \left(\frac{\frac{q}{A}}{T - T_{\mathrm{ref}}} \right) \frac{\delta x}{K} \tag{21}$$

where q is the heat transfer rate, δx – the distance from the surface boundary to the nearest local point. The mean Nusselt number along the heated vertical wall is deduced through the expression:

$$\overline{\mathrm{Nu}} = -\frac{\int_0^H \mathrm{Nu}\,\mathrm{d}y}{H} \tag{22}$$

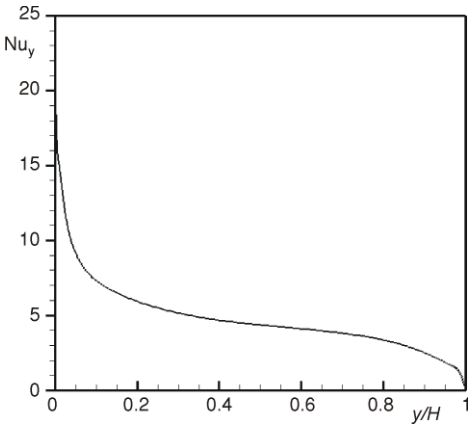

Figure 7. Local Nusselt number along the hot wall deduced by SST *k-ω* model, Ra =1.43·10^6

Figure 7 shows the local Nusselt number deduced by the SST *k-ω* model along the hot wall. This figure evidences that the evolution of Nusselt number along the heated wall has not the transition zone, and this confirms that the interaction between the both outer layers, which will generate a vertical stratification will prevent the transition to turbulent flow.

The different values of the average Nusselt number along the hot wall for the both models (SST and RNG models), experimental value [9] and the numerical results for Hsieh *et al.* [10] are summarised in tab. 3. Heish *et al.* [10] used an unsteady RANS approach combined with low-Re *k-ε* model of Lien *et al.* [29] for the 2-D flow simulation in the tall cavity with aspect ratio *Ar* = 28.68. They concluded that the steady RANS can be used to compute this flow without countering convergence problems. Table 3 shows that the better predictions are obtained by the SST *k-ω* model, especially for low Rayleigh number cases. Nevertheless, the difference still not significant compared to the RNG *k-ε* model.

Table 3. Mean Nusselt number near the hot wall for high and low Rayleigh numbers; in brackets the error compared to experiment results

	$\overline{\mathrm{Nu}}$ (low Ra)	$\overline{\mathrm{Nu}}$ (high Ra)
Experiment [9]	5.85	7.57
Numerical results [10]	–	6.39 (15.59%)
Numerical results for RNG model	5.51 (5.81%)	6.905 (8.78%)
Numerical results for SST model	5.66 (3.25%)	6.96 (8.06%)

Generally, the heat transfer depends on the Rayleigh number, Prandtl number, and the aspect ratio as: Nu = *f*(Ra, Pr, *Ar*). In this work, the Prandtl number is almost constant within the range of the considered temperature variation and the dimensions of the cavity are constant. So, we have just to examine the variation of the average Nusselt number *vs.* the Rayleigh number.

In order to correlate this variation, different differential temperatures between the two vertical plates have been applied (tab. 4.). In this part, only the SST *k-ω* model has been considered in the simulations. For natural convection, MacGregor *et al.* [17], Henkes *et al.* [30], and Dafa'alla *et al.* [15] measure the flow within different cavities sizes; all gave an averaged wall-heat transfer correlation by a power law expression:

$$\overline{\mathrm{Nu}} = c\sqrt[3]{\mathrm{Ra}} \tag{23}$$

where the constant *c* is somewhat different (*c* = 0.046, 0.047, and 0.053).

Conversely, for large aspect ratios and for moderate Rayleigh number:

– MacGregor *et al.* [16, 17] proposed the following correlations:

$$\overline{\mathrm{Nu}} = 0.42\sqrt[4]{\mathrm{Ra}}\,\mathrm{Pr}^{0.012}\left(\frac{H}{W}\right)^{-0.3} \quad \text{for} \quad \begin{bmatrix} 10 \le Ar \le 40 \\ 1 \le \mathrm{Pr} \le 2\cdot 10^4 \\ 10^4 \le \mathrm{Ra} \le 10^7 \end{bmatrix} \tag{24a}$$

$$\overline{\mathrm{Nu}} = 0.046\sqrt[3]{\mathrm{Ra}} \ \text{ for } \begin{bmatrix} 1 \le Ar \le 40 \\ 1 \le \mathrm{Pr} \le 20 \\ 10^6 \le \mathrm{Ra} \le 10^9 \end{bmatrix} \tag{24b}$$

– When a cavity is heated at a fixed temperature (isothermally) from the sides, correlation equation for the Nusselt number relation in the turbulent regime, based on experimental data, has been proposed by El Sherbiny *et al.* [20]:

$$\begin{aligned} &\mathrm{Nu}_1 = 0.0605\sqrt[3]{\mathrm{Ra}} \\ &\mathrm{Nu}_2 = \sqrt[3]{1+\frac{0.104\,\mathrm{Ra}^{0.293}}{1+\left(\frac{6310}{\mathrm{Ra}}\right)^{1.36}}} \quad \text{For } 5 \le Ar \le 110 \\ &\mathrm{Nu}_3 = 0.242\left(\frac{\mathrm{Ra}}{Ar}\right)^{0.272} \quad \text{Air} \\ &\mathrm{Nu} = \max.(\mathrm{Nu}_1, \mathrm{Nu}_2, \mathrm{Nu}_3) \quad \begin{pmatrix} Ar = 20 : \mathrm{Ra} < 2\cdot 10^6 \\ Ar = 40 : \mathrm{Ra} < 2\cdot 10^5 \\ Ar = 80 : \mathrm{Ra} < 3\cdot 10^4 \end{pmatrix} \end{aligned} \tag{25}$$

Figure 8 shows the variation of Nu *vs.* Ra obtained by this present numerical study (tab. 4), experimental results [9], MacGreror correlations (eq. 24), and El Sherbiny correlation (eq. 25). We observe in fig. 8. that the MacGregor correlations underestimate the Nu compared to the experimental data and numerical results, because the correlations proposed is for $\mathrm{Pr} \geq 1$. While, the Nu evolution shows a good agreement with the experimental results of

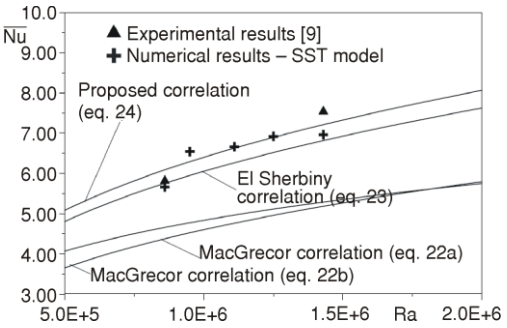

Figure 8. Profile of the average Nusselt number *vs.* the Rayleigh number

El Sherbiny (Nu_1). However, the El Sherbiny correlation (eq. 25.) shows that when *Ar* increases the range of Rayleigh number should decrease. Therefore, the fig. 8. shows that the Sherbiny correlation tends to underestimate the Nu number when the Rayleigh number increases.

Consequently, according to eqs. 24(b) and 25, and after fitting, respectively, by a quadratic interpolation, a new correlation (fig. 8) is proposed for air and for high aspect ratio:

$$\overline{\mathrm{Nu}} = 0.0635\sqrt[3]{\mathrm{Ra}} \tag{26}$$

Table.4. Average Nusselt number by SST *k-ω* model for different Rayleigh numbers

Ra	8.6E+5	9.5E+5	1.11E+6	1.25E+6	1.43E+6
$\overline{\mathrm{Nu}}$	5.66	6.54	6.66	6.92	6.96

Conclusions

In this work, a 3-D numerical study has been investigated using two one-point closure turbulence models: RNG *k-ε* and SST *k-ω* models. The numerical results are compared to the experimental data of Betts and Bokhari for the air turbulent natural convection.

A good agreement between the experimental and numerical prediction is observed for both RNG *k-ε* model and SST *k-ω* model. However, for more accuracy the better results were obtained by using SST *k-ω* model. The profiles of the mean vertical velocity, mean temperature, and the turbulent kinetic energy denote that the flow in the core region of the tall cavity is very weak and the turbulence level increases with Rayleigh number.

Accordingly, where the motion occurs, the iso-surface vorticity highlighted a stretched vortex along the tall cavity and two small scales vortex close to the cavity corners. The stretched vortex increases in magnitude and in scale when Rayleigh increases.

Finally, the correlations between the Rayleigh number and the Nusselt number is underestimate by MacGregor correlations whereas the experimental results of El Sherbiny provide a good correlation. However, for aspect ratio *Ar* = 28.6, when the Ra number increases, El Sherbiny correlation becomes to underestimate the experimental results.

In this paper, a new correlation is proposed for natural convection air flow in an enclosed tall cavity with high aspect ratio.

Nomenclature

a – thermal diffusivity, [m^2s^{-1}]
Ar – cavity aspect ratio, [–]
C_p – specific heat, [$Jkg^{-1}K^{-1}$]
D – depth of the cavity, [m]
H – height of the cavity, [m]
K – thermal conductivity, [$WK^{-1}m^{-1}$]
k – turbulent kinetic energy, [m^2s^{-2}]
Nu – Nusselt number, [–]
Pr – Prandtl number, [–]
Ra – Rayleigh number, [–]

Re – Reynolds number, [–]
R_{ij} – Reynolds stress tensor, [kgm^{-1}s^{-3}]
S – modulus of the mean rate-of-strain tensor, [s^{-1}]
T – temperature, [K]
T_0 – operating temperature, [K]
T_{ref} – Reference temperature, [K]
v_y – vertical velocity, [ms^{-1}]
W – width of the cavity, [m]

Greek symbols

α_t – Eddy diffusivity, [m^{2}s^{-1}]
β – Thermal expansion coefficient, [K^{-1}]
δ_{ij} – Kronecker symbol
ε – turbulent energy dissipation rate, [m^{2}s^{-3}]
κ – thermal conductivity, [Wm^{-1}K^{-1}]
μ – dynamic viscosity, [kgm^{-1}s^{-1}]
μ_{eff} – effective viscosity, $\mu_{\text{eff}} = \mu + \mu_t$
μ_t – eddy viscosity, [kgm^{-1}s^{-1}]
ν – kinematics viscosity, [m^{2}s^{-1}]
ρ – fluid density, [kgm^{-3}]
σ_k – turbulent Prandtl number for k, [–]
σ_t – turbulent Prandtl number, [–]
σ_ε – turbulent Prandtl number for ε, [–]
σ_ω – turbulent Prandtl number for ω, [–]
τ_{ij} – viscous stress tensor, [m^{2}s^{-2}]
Ω – vorticity magnitude, [s^{-1}]
ω – turbulent frequency, [s^{-1}]

Subscripts and superscripts

c, h – cold, hot wall
m – mean value
RNG – constants for the RNG k-ε model
t – turbulent
$^-$ – average value

References

[1] Aksouh. M., *et al*. Assessment of Performance of Low Reynolds Turbulence Models in Predicting Natural Convection. ECCOMAS, *Proceedings on CD*, 5th European Conference on Computational Fluid Dynamics, Lisbon, 2010
[2] Peng, S., Davidson, L., Large Eddy Simulation for Turbulent Buoyant Flow in a Contained Cavity, *Int. J. Heat Mass Transfer, 22* (2001), 3, pp. 323-331
[3] Tian, Y. S., Karayiannis, T. G., Low Turbulence Natural Convection in an Air Filled Square Cavity, Part I: The Thermal and Fluid Flow Fields, *Intr. Comm. in Heat and Mass Transfer, 43* (2000), 6, pp. 849-866
[4] Salat, J., *et al*., Experimental and Numerical Investigation of Turbulent Natural Convection in a Large Air-Filled Cavity, *International Journal of Heat and Fluid Flow, 25* (2004), 5, pp. 824-832
[5] Gustaven, A. Thue, J. V., Numerical Simulation of Natural Convection in Three-Dimensional Cavities with a High Vertical Aspect Ratio and Low Horizontal Aspect Ratio, *Journal of Building Physics, 30* (2007), 3, pp. 217-240
[6] Yang, H., Zhu, Z., Numerical Study of Three-Dimensional Turbulent Natural Convection in a Differentially Heated Air-Filled Tall Cavity. *Intr. Comm. in Heat and Mass Transfer, 35* (2008), 5, pp. 606-612
[7] Pons, M., Transition from Single to Multi-Cell Natural Convection of Air in Cavities with Aspect Ratio of 20: A Thermodynamic Approach, *Int. J. of Thermodynamics, 11* (2008), 2, pp. 71-79
[8] Aich, W., Hajri, I., Omri, A., Numerical Analysis of Natural Convection in a Prismatic Enclosure, *Thermal Science, 15* (2011), 2, pp. 437-446
[9] Betts, P. L., Bokhari, I. H., Experiments on Turbulent Natural Convection in an Enclosed Tall Cavity, *Intr. J. of Heat and Fluid Flow, 21* (2000), 6, pp. 675-683
[10] Hsieh, K. J., Lien, F. S., Numerical Modelling of Buoyancy-Driven Turbulent Flows in Enclosures, *Intr. J. of Heat and Fluid Flow, 25* (2004), 4, pp. 659-670
[11] Aksouh, M., Mataoui, A., Numerical Study of the Turbulent Natural Convection in an Enclosed Tall Cavity for the High and Low Rayleigh Number, ACOMEN Advanced Computational Methods in Engineering, Liege, Belgium, 2008
[12] Yakhot, V., Orszag, S. A., Renormalization Group Analysis of Turbulence, *Journal of Scientific Computing, 1* (1986), 1, pp. 3-51
[13] Menter, F. R., Two-Equation Eddy-Viscosity Turbulence Models for Engineering Applications, *AIAA Journal, 32* (1994), 8, pp. 1598-1605
[14] Cuypers, Y, Maurel, A., Petitjeans, P., Characterization of a Turbulent Vortex using Phase Averaged PIV Data, *Progress in Turbulence II* , (Eds. M. Oberlack *et al*.), *Springer Proceedings in Physics, 109* (2007), 2, pp. 65-70

[15] Dafa'Alla, A. A., Betts, P. L., Experimental Study of Turbulent Natural Convection in a Tall Air Cavity, *Exp. Heat Transfer, 9* (1996), 2, pp. 165-194
[16] Incropera, F. P., *et al.*, Fundamental of Heat and Mass Transfer, 6th ed., John Wiley and Sons, New York, USA, 2007
[17] MacGregor, R. K., Emery, A. P., Free Convection through Vertical Plane Layers: Moderate and High Prandtl Number Fluids, *ASME J. Heat Transfer, 91* (1969), 3, pp. 391-403
[18] Ouriemi, M., Vasseur, P., Bahloul, A., Natural Convection of a Binary Mixture Confined in a Slightly Inclined Tall Enclosure, *Intr. J. of Heat and Mass Transfer, 32* (2005), 6, pp. 770-778
[19] Xaman, J. *et al*., Numerical Study of Heat Transfer by Laminar and Turbulent Natural Convection in Tall Cavities of Façade Elements, *Energy and Buildings, 37* (2005), 7, pp. 787-794
[20] Elsherbiny, S. M., Raithby, G. D., Hollands, K. G. T., Heat Transfer by Natural Convection Across Vertical and Inclined Air Layers, *Trans. ASME J. Heat Transf., 104* (1982), 1, pp. 96-102
[21] Wilcox, D. C., Turbulence Modelling for CFD, DCW Industries Inc., La Canada, Cal., USA, 1994
[22] Patankar, S. V., Numerical Heat Transfer and Fluid Flow, Series in Computational Methods in Mechanics and Thermal Sciences, Hemisphere Publishing Corp. & Mc Graw Hill, New York, USA, 1981
[23] Aounallah, A., *et al*., Numerical Investigation of Turbulent Natural Convection in an Inclined Square Cavity with a Hot Wavy Wall, *Intr. J. of Heat and Mass Transfer, 50* (2007), 9-10, pp. 1683-1693
[24] El Gharbi *et al.*, An Improved Near-Wall Treatment for Turbulent Channel Flows, *Inter J of Comput. Fluid Dynamics, 25* (2001), 1, pp. 41-46
[25] Ampofo, F., Karayiannis, T. G., Experimental Benchmark Data for Turbulent Natural Convection in an Air Filled Square Cavity, *Intr. J. of Heat and Mass Transfer, 46* (2003), 19, pp. 3551-3572
[26] Bennacer, R., *et al*., Generalisation of Two-Layer Turbulent Model for Passive Cooling in a Channel, Tokyo JSME, 11th International Conference on Nuclear Engineer, Tokyo, 2003, No. 03-209
[27] Foias, C. *et al*., Navier-Stokes Equations and Turbulence, Book Cambridge University Press, Cambridge, UK, 2004
[28] Kemenov, K. A., New Two-Scale Decomposition Approach for Large-Eddy Simulation of Turbulent Flows, Ph. D. thesis, School of Aerospace Engineering, Georgia Institute of Technology, Atlanta, Geo., USA, 2006
[29] Lien, F. S., Leschziner, M. A., Computational Modelling of a Transitional 3D Turbine-Cascade Flow Using a Modified Low-Re k–ε Model and a Multi-Block Scheme, *Inter. J. of Comp. Fluid Dynamics, 12* (1999), 1, pp. 1-15
[30] Henkes, R. A. W. M., Vander Flugt, F. F., Hoogendoorn, C. J., Natural Convection Flow in a Square Cavity Calculated with Low-Reynolds-Number Turbulence Models, *Intr. J. of Heat and Mass Transfer, 34* (1991), 2, pp. 377-388

Paper submitted: February 1, 2011
Paper revised: October 3, 2011
Paper accepted: October 8, 2011